Biochimica et Biophysica Acta 1834 (2013) 87–97

Contents lists available at SciVerse ScienceDirect

Biochimica et Biophysica Acta

journal homepage: www.elsevier.com/locate/bbapap

Biophysical characterization of higher plant Rubisco activase

J. Nathan Henderson [a], Suratna Hazra [a], Alison M. Dunkle [a], Michael E. Salvucci [b], Rebekka M. Wachter [a,*]

[a] Department of Chemistry and Biochemistry, Arizona State University, Tempe, AZ 85287, USA
[b] US Department of Agriculture-Agricultural Research Service, Arid-Land Agricultural Research Center, Maricopa, AZ 85138, USA

ARTICLE INFO

Article history:
Received 1 August 2012
Received in revised form 7 September 2012
Accepted 9 September 2012
Available online 14 September 2012

Keywords:
Rubisco regulation
Protein assembly
Quaternary structure
Protein aggregation
Thermostability
Polydispersity

ABSTRACT

Rubisco activase (Rca) is a chaperone-like protein of the AAA+ family, which uses mechano-chemical energy derived from ATP hydrolysis to release tightly bound inhibitors from the active site of the primary carbon fixing enzyme ribulose 1,5-bisphosphate oxygenase/carboxylase (Rubisco). Mechanistic and structural investigations of Rca have been hampered by its exceptional thermolability, high degree of size polydispersity and propensity towards subunit aggregation. In this work, we have characterized the thermal stability and self-association behavior of recombinant Rca preparations, and have developed ligand screening methods. Thermal denaturation profiles generated by circular dichroism indicate that creosote and tobacco short-form Rcas are the most stable proteins examined, with an estimated mid-point temperature of 45–47 °C for protein denaturation. We demonstrate that ADP provides a higher degree of stabilization than ATP, that magnesium ions have a small stabilizing effect on ATP-bound, but a significant destabilizing effect on ADP-bound Rca, and that phosphate provides weak stabilization of the ADP-bound form of the protein. A dimeric species was identified by size-exclusion chromatography, suggesting that the two-subunit module may comprise the basic building block for larger assemblies. Evidence is provided that chromatographic procedures reflect non-equilibrium multimeric states. Dynamic light scattering experiments performed on nucleotide-bearing Rca support the notion that several larger, highly polydisperse assembly states coexist over a broad concentration range. No significant changes in aggregation are observed upon replacement of ADP with ATP. However, in the absence of nucleotides, the major protein population appears to consist of a monodisperse oligomer smaller than a hexamer.

1. Introduction

Rubisco (ribulose 1,5-bisphosphate carboxylase/oxygenase) is a key photosynthetic enzyme responsible for the incorporation of atmospheric carbon dioxide into ribulose bisphosphate (RuBP). This process generates the necessary building blocks for carbohydrate biosynthesis [1]. In higher plants, the activation state of Rubisco is strictly dependent on Rubisco activase (Rca) activity. Several turnover-dependent processes of Rubisco have been linked to the production of competitive inhibitors, and these inhibitors reduce the fraction of Rubisco sites that are catalytically competent. In addition, decarbamylation of an active site catalytic lysine has been shown to lead to the formation of inhibited complexes through the binding of RuBP [2,3]. Rca utilizes ATP hydrolysis to mechanically modify the conformation of Rubisco to release tight-binding inhibitors. Inhibition of Rca activity has been linked to the temperature-dependent loss of carbon fixation in higher plants [4–7]. Primarily, the Rca-mediated reactivation process involves Rubisco conformational rearrangements of a large subunit loop region and a C-terminal peptide that are packed over inhibited sites [3,8]. Coupled to these events is a subtle N-domain motion that is associated with additional geometric changes around the active sites of Rubisco [9].

Two isoforms of Rca have been characterized, long-form α (46 kDa) and short-form β (42 kDa) Rca [10]. The ATPase activity of both forms is thought to be regulated by the ambient ADP/ATP ratio, which is a function of the stromal energy charge. Consistent with ADP inhibition, the dissociation constants for the ATP substrate and the ADP product have been estimated to lie in the low-micromolar and high nano-molar range respectively [11]. For the longer α-Rcas, the regulation by the adenylate pool is affected by the environmental redox status, as mediated by two C-terminal cysteine residues that are part of the long-form C-extension [12–14].

In higher plants, moderate heat stress is known to cause a substantial decrease in net photosynthetic rates [5,15,16]. At elevated temperatures, Rubisco activity is substantially reduced, and this effect has been linked to the inhibition of Rubisco reactivation. Therefore, diminished Rca activity has been proposed to play a critical role in heat-related limitations of net photosynthesis [5]. In vitro, Rca was reported to lose ATPase activity at temperatures slightly above the

Abbreviations: Rubisco, ribulose-1,5-bisphosphate carboxylase/oxygenase; Rca, Rubisco activase; RuBP, ribulose bisphosphate; SE, size exclusion; HPLC, high pressure liquid chromatography; DLS, dynamic light scattering; CD, circular dichroism; Pd, polydispersity; R_h, hydrodynamic radius; D, diffusion coefficient

* Corresponding author at: Department of Chemistry and Biochemistry, Arizona State University, Tempe, AZ 85287-1604, USA. Tel.: +1 480 965 8188; fax: +1 480 965 2747.
E-mail address: rwachter@asu.edu (R.M. Wachter).

1570-9639/$ – see front matter © 2012 Elsevier B.V. All rights reserved.
http://dx.doi.org/10.1016/j.bbapap.2012.09.006

thermal optimum for plant growth [5,17], and Rca inactivation was shown to be accompanied by protein aggregation [13]. The temperature optimum for ATP hydrolysis was reported to be 8 to 10 °C higher for proteins from warm-climate plants (creosote, cotton and tobacco Rca) compared to proteins from cold-climate plants (Antarctic hair grass and spinach Rca) [17]. In vitro studies involving recombinant *Arabidopsis thaliana* Rca demonstrated that 0.5 mM ADP provided significant protection against thermal inactivation, an effect that was counteracted by magnesium ion concentrations that exceeded nucleotide concentrations by 1.5 and 4.5 mM [13].

Rca belongs to the superfamily of AAA+ P-loop ATPases, ring-forming motor proteins that utilize the chemical energy of ATP hydrolysis to carry out mechanical work on DNA or protein substrates [18–20]. Both domains of the AAA+ module (200–250 amino acids) contribute to nucleotide binding near the hinge region [21–23], and individual subunits are known to form ring-like assemblies that operate by means of allosteric regulation [24–26]. Recently, two Rca X-ray structures have become available, a 1.9 Å model of the creosote C-domain (residues 250–351 out of 379 total) [27], and a 3.0 Å model of the tobacco AAA+ domain (residues 68–360 out of 383 total) [28] (Fig. 1). The two models suggest conformational plasticity in the specificity-determining region shown to be responsible for differentiation between *Solanaceae* and non-*Solanaceae* Rubiscos [29]. The tobacco apo-protein crystallized in a pseudo-hexameric spiral, such that closed-ring toroidal models could be generated by fitting into negative stain electron microscopy (EM) maps (Fig. 1). Mutagenesis data suggested that loop regions lining the central pore play important roles in ATP hydrolysis and Rubisco reactivation. However, the macromolecular surfaces involved in the physical interaction of Rca with Rubisco remain poorly determined [28].

Although Rca-mediated reactivation of Rubisco can be reconstituted in the test tube [5], the Rca self-association behavior responsible for generating active assemblies remains poorly understood. Regardless, known assembly mechanisms of other AAA+ proteins can be utilized to delineate possible Rca subunit interaction modes. Frequently, AAA+ assemblies involve hexameric toroids, especially within the classic clade that includes Rca [23]. Some members of this clade have been reported to require specific factors to form functional oligomers, such as the katanin dimer, which utilizes microtubules as templates for additional assembly, but only in the presence of ATP [30]. In other instances, nucleotides modulate the interactions with oligomeric partner proteins, such as in the proteasomal ATPase [26]. A number of protein families (e.g. Cdc48/p97/VCP and ClpABC) consist of tandem arrays of AAA+ domains termed D1 (classic clade) and D2 (clade 5), such that two hexameric rings are stacked on top of each other [31]. Along these lines, a well-studied example is ClpA, where D1 hexamerization is ATP- and Mg^{2+}-dependent and includes a tetramer–hexamer equilibrium with a K_d value less than 0.17 nM [32]. Overall, obligate hexamers are most commonly observed, and the formation of a six subunit toroidal ring appears to be the default state within the classic clade of AAA+ proteins.

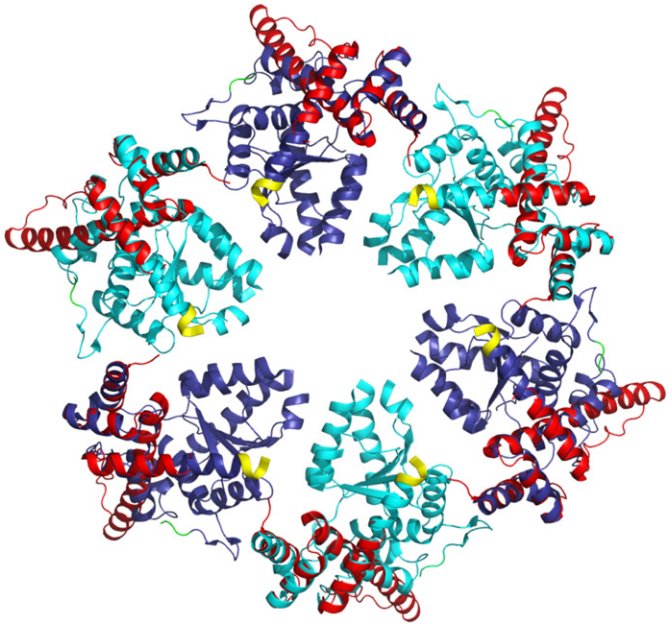

Fig. 1. Hexameric model of the tobacco Rca apo-AAA+ domain (residues 69–360) with superposed creosote recognition domain (residues 250–351). Tobacco: blue and cyan with yellow C-termini [28]; creosote: red [27].

Contrary to other AAA+ modules, the oligomeric stoichiometry of higher plant Rca has been surprisingly difficult to characterize. A high degree of size polydispersity has been described in most Rca preparations, and oligomeric molecular weight estimates reported in the literature have ranged from 58 to well over 550 kDa based on size-exclusion HPLC (SE-HPLC) [6,13,33]. In these studies, a strong dependence on protein concentration and other assay conditions has been observed (ATP, ATP-γ-S, Mg^{2+}, ADP, apo-form, polyethylene glycol, ionic strength, glycerol, temperature). SE-HPLC elution profiles have been reported to consist of broad bands with long, trailing downslopes, indicative of binding equilibria comprising a large number of subunit stoichiometries [6]. Nucleotides have been demonstrated to promote self-association [6], whereas the apo-protein was reported to be highly thermolabile [13].

Recently, a few site-directed Rca mutants have allowed for a more precise characterization of oligomeric states. In the tobacco Rca-R294A variant, a subunit–subunit interaction is disrupted, such that hexameric structures could be identified by high-resolution mass spectrometry in the presence of ATP-γS [34]. Subsequently, tobacco Rca-R294V was reported to be fully active and yield hexameric assemblies in EM reconstructions [28]. As before, a 6-fold symmetry was observed solely in the presence of ATP and ATP-γS, whereas amorphous particles seemed to form in the presence of ADP [28]. However, the assembly process for wild-type Rca and the role of different nucleotides in self-association remain poorly understood.

The mechanistic enzymology of Rca ATPase and Rubisco remodeling activities is of intense current interest, as these processes regulate the extent of atmospheric carbon fixation. Any protein engineering effort to improve the functioning of Rubisco-Rca pairs must take into account Rca thermostability and its proper assembly into productive oligomers. To better understand thermal effects on activity loss as a function of plant environmental acclimation, we have examined species differences in Rca denaturation profiles by circular dichroism (CD), and have identified biologically relevant ligand conditions that stabilize the protein fold. To better understand the dynamics of Rca subunit assembly into functional multimers, we have developed affinity purification protocols to obtain homogeneous protein preparations, and have examined the Rca self-association behavior using SE-HPLC and dynamic light scattering (DLS).

2. Materials and methods

2.1. Heterologous protein expression and purification Rca in the absence of an affinity tag

Rca proteins bearing an N-terminal methionine residue but no fusion tag consisted of the spinach (*Spinacia oleracea*) α-form, the *A. thaliana* β-form, the cotton (*Gossypium hirsutum*) β-form, tobacco (*Nicotiana tabatum*), and creosote (*Larrea tridentata*) α- and β-forms. These proteins were expressed in *E. coli* and purified by procedures described previously [14]. Briefly, the *E. coli* strain BL21(DE3)pLysS was transformed with a pET-23a or d(+) vector (EMD Chemicals/Novagen) bearing cDNA coding for mature Rca. Liquid cultures were induced with IPTG, protein was expressed at 25 °C, cells were harvested by centrifugation and ruptured by sonication. The purification procedure involved an

ammonium sulfate precipitation step (37.5% ammonium sulfate), followed by ultracentrifugation to remove membrane vesicles. Subsequently, the sample was further purified by gel filtration, followed by anion exchange using a Q-Sepharose Hi-Trap column and a potassium chloride step gradient. Once purified to homogeneity, protein preparations were flash-frozen and stored at −80 °C [14].

2.2. Cloning of 6His-tagged cotton β-Rca

A blunt-ended PCR product comprising 1144 base pairs was amplified from a pET23a(+) expression plasmid containing full-length cotton β-Rca with a C-terminal Ala-Cys insert after residue 378 of the 380-residue protein [35]. The 50 μL PCR reaction contained 20 ng plasmid, 0.625 U Pfu Turbo DNA polymerase (Stratagene), 1x Cloned Pfu DNA polymerase reaction buffer (Stratagene), 125 μM of each dNTP (Invitrogen) and 5 pmol of forward and reverse primers (Integrated DNA Technologies) with the following sequences: 5′-CACCATGGCCAAA GAGATAG-3′ and 5′-TTAGAACGCACAAGCTCC-3′, respectively. Blunt-ended PCR product amplification, directional "TOPO" cloning of the blunt-ended PCR product into a linear pET151/D-TOPO vector (Invitrogen), and subsequent transformation into One Shot TOP10 competent cells (Invitrogen) were carried out according to the manufacturer's recommendations. Plasmid was prepared from individual transformant colonies using the QIAprep Spin Miniprep Kit (Qiagen), and the correct insert was verified by sequencing at the Arizona State University School of Life Sciences DNA Laboratory.

2.3. Expression and affinity-purification of 6His-tagged cotton β-Rca

A pET151/D-TOPO vector containing cotton β-Rca was transformed into *E. coli* BL21 Star (DE3) cells (Invitrogen), single colonies of which were cultured overnight in 125 mL baffled Erlenmeyer flasks containing 25 mL of Luria-Bertani (LB) media supplemented with a 100 μg/mL carbenicillin. After shaking overnight at 250 rpm and 37 °C, these cultures were used to inoculate 1 L LB plus 100 μg/mL carbenicillin cultures contained in 2.8 L Fernbach flasks. Growth was continued at 250 rpm and 37 °C until the OD_{600} of the cultures reached ~0.6. The cultures were then cooled to ~25 °C, 100 mg of isopropyl-β-D-thio-galactoside (IPTG) was added to each flask, and growth continued at 200 rpm and 25 °C. After 8 h, the cultures were harvested by centrifugation and the cell pellets were frozen at −80 °C. Thawed cell paste was resuspended in 50 mL of 25 mM 4-(2-hydroxyethyl)-1-piperazineethanesulfonic acid (HEPES) pH 8.0, 20 mM imidazole pH 8.0, 300 mM NaCl, 10% glycerol, 1 mM ethylenediaminetetraacetic acid (EDTA), 1 mM phenylmethanesulfonylfluoride, 1 mM dithiothreitol (DTT), 0.5 mM adenosine diphosphate (ADP) and 0.1% Triton X-100, then disrupted by sonication. For preparation of apo cotton β-Rca, ADP was omitted from all buffers. The lysate was pelleted by centrifugation to remove insoluble material and the supernatant was passed through a 0.8 μm syringe filter before being loaded on to a Ni-NTA column (Qiagen). Cotton β-Rca was purified using an imidazole buffer step gradient (25 mM HEPES pH 8.0, 300 mM NaCl, 1 mM DTT and 0.5 mM ADP with variable amounts of imidazole at pH 8.0). The column was first washed with 5 column volumes (25 mL) of 50 mM imidazole buffer and followed with 25 mL of 100 mM imidazole buffer. His-tagged cotton β-Rca was eluted from the column in 25 mL of 500 mM imidazole buffer wash. Fractions containing the His-tagged protein were pooled, 1.2 mg of tobacco etch virus protease (TEV) was added to the fractions to remove the His-tag, and the entire sample was dialyzed overnight at 10 °C against 1 L of 25 mM 2-amino-2-hydroxymethyl-propane-1,3-diol (Tris) pH 8.0, 300 mM NaCl, 0.1 mM ADP, 0.1 mM DTT and 1 mM EDTA. The dialysate was reapplied to a Ni-NTA column (Qiagen), and the TEV-cleaved cotton β-Rca was collected in the flowthrough and low imidazole fractions (20 mM). Protein was concentrated in Centriprep centrifugal concentrators (Millipore) to a volume of ~2.5 mL. The buffer was exchanged into 25 mM HEPES pH 7.5, 300 mM KCl, 2 mM ADP and 10% glycerol using a PD-10 column (GE Healthcare). Protein concentration was then measured using the Bradford method with typical yields of 2–3 mg of protein per liter of cell culture. Aliquots were frozen under liquid nitrogen and stored at −80 °C. Prior to preparation for the Thermofluor assay, cotton β-Rca samples were buffer exchanged into 25 mM HEPES pH 7.5 and 150 mM KCl by gel filtration through 2 mL Sephadex G-50 columns [36].

2.4. Size-exclusion high-pressure liquid chromatography (SE-HPLC)

Rca preparations were analyzed by SE-HPLC using a Biosep S-4000 (Phenomenex) column (600 × 7.8 mm, resolving range from 15,000 to 1,500,000 Daltons). The mobile phase consisted of either 25 mM HEPES pH 7.5, 250 mM KCl, 10% glycerol and 0.1 mM ADP, or 50 mM phosphate pH 7.2, 1 mM $MgSO_4$ and 0.1 mM ADP. The flow rate was adjusted to 0.8 ml/min and elution was monitored by absorbance at 280 nm. Standard curves were generated for each of the two mobile phases, using thyroglobulin (670 kDa), γ-globulin (158 kDa), ovalbumin (44 kDa), myoglobin (17 kDa), *A. thaliana* Rubisco (585 kDa), and GFP (28.3 kDa) as protein standards. Blue dextran (~2000 kDa) and Vitamin B12 (1.35 kDa) served as high- and low-MW species to determine the fully excluded (V_o) and fully included (V_t) volumes of the column. These values were utilized to normalize the sample elution volume V_e based on the resolving range of the column according to the equation $K_{av} = (V_e - V_o)/(V_t - V_o)$. Standard curves were generated by graphing log (MW) vs. K_{av}, and utilized to estimate the MW of Rca preparations. The standard curves for each of the two mobile phases were essentially identical. Error estimates in mass determinations were carried out by comparing the mass determined by SE-HPLC with the known mass of several protein standards (thyroglobulin, γ-globulin, ovalbumin, myoglobin, Rubisco, and GFP). The error associated with mass determinations ranged from 20 to 30%, and clustered around a 25% relative standard error.

Samples of *A. thaliana* β-Rca-Y53A were prepared by serial dilution of an 11 mg/ml sample (260 μM) using buffer consisting of 50 mM HEPES pH 7.2, 20 mM NaCl, 1 mM $MgCl_2$ and 0.1 mM ADP. Upon dilution, each sample was incubated at 4 °C for one hour, followed by injection of 100 μl into the HPLC system at a protein concentration of 260, 130, 65, 6.5 and 0.65 μM. For the 260-μM sample (Fig. 2A, green chromatogram), four 0.5-min fractions of the main elution band were hand collected (one fraction for the upslope, and three fractions for three-quarters of the downslope), and 100 μl of each collected fraction was re-injected into the HPLC system on the same day (Fig. 2B). Molecular mass estimates were carried out for the peak positions of each eluting band using the standard curves described above. In another set of experiments, on-column dilution was examined by determining the protein concentration of the eluting peak fraction by the Bradford method, and comparing the concentration with the estimated molecular weight at the peak position (Fig. 2C).

2.5. Circular dichroism (CD) spectroscopy

To buffer-exchange samples and increase homogeneity, Rca preparations were injected into the SE-HPLC system immediately prior to CD measurements. To this end, the HPLC system was equilibrated in a mobile phase consisting of 50 mM phosphate pH 7.2, 1 mM $MgSO_4$ and 0.1 mM ADP. For each experiment, 100 μl of 2 to 6 mg/ml Rca were injected, and 1.6 ml of the apex of the eluting band (2 min collection time) was collected and subsequently utilized for CD experiments. The elution volume of the collected sample was consistent with protein complexes ranging from about 10 to 70 subunits (~3 MDa).

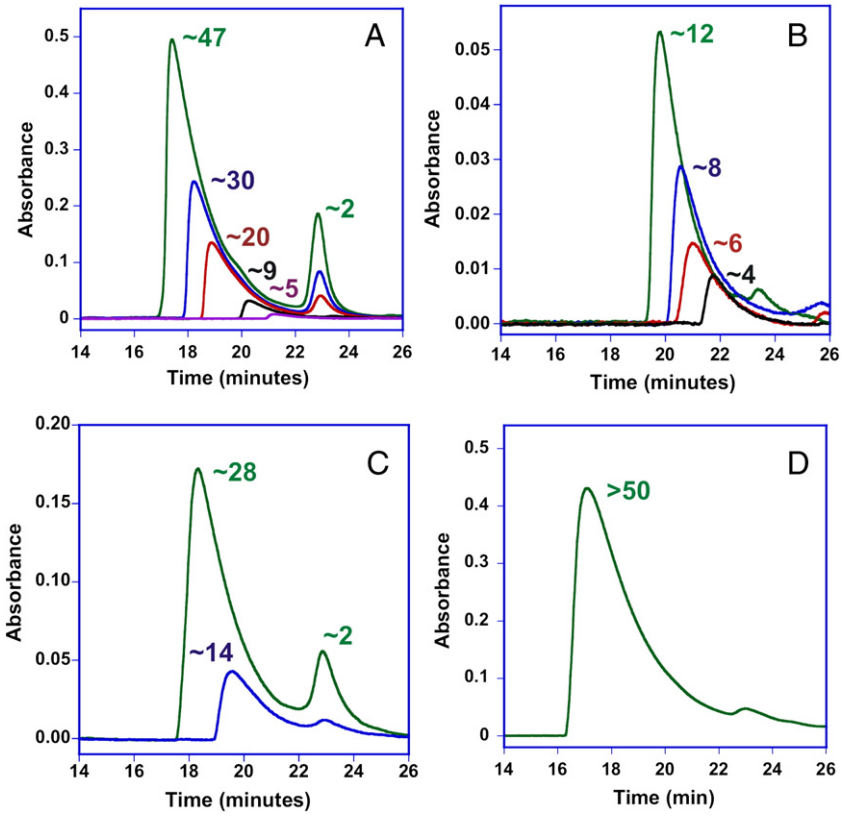

Fig. 2. Size-exclusion chromatograms collected on different Rca preparations. Approximate subunit stoichiometries at the peak positions are indicated. A. Arabidopsis Rca subunit concentrations as injected (100 μl volume): 260 μM (green), 130 μM (blue), 65 μM (red), 6.5 μM (black), 0.65 μM (purple). B. Re-injected Arabidopsis Rca fractions collected from chromatogram A as described in the text. Green: ~12-mer (reinjection of ~47-mer); blue: ~8-mer (reinjection of putative 40-mer); red: ~6-mer (reinjection of putative 30-mer); black: ~ 4-mer (reinjection of putative 20-mer). C. Arabidopsis Rca; green: 260 μM (50 μl volume); blue: 26 μM (50 μl); concentrations of eluted peak fractions: 13 μM (green) and 1.3 μM (blue). D. Tobacco Rca, 140 μM (100 μl); peak fractions utilized for CD experiments.

Samples were analyzed on a Jasco J-710 circular dichroism spectropolarimeter with a thermoelectric temperature controller (Jasco-PTC-424S). CD scans as a function of wavelength were acquired from 180 to 260 nm using a quartz cuvette (Helma; path length 1 mm) at a scan rate of 50 nm/min, a band width of 2 nm, a data pitch of 0.5 nm, and a response time of 1 s. Three accumulations were carried out per data point. If the signal amplitude exceeded 20 mdeg at any wavelength, the sample was diluted with 50 mM phosphate pH 7.2, 1 mM $MgSO_4$ and 0.1 mM ADP. For CD measurements as a function of temperature, the sample cell was heated at a rate of 1 deg/min, and wavelength scans were collected at 15, 25, 35, 45, 55, and 65 °C while keeping the temperature constant. In addition, the ellipticity at 208 nm (3 accumulations) was determined at 20, 30, 40, 50, and 60 °C. Wavelength scans were also collected on an appropriate buffer blank and subtracted from protein spectra. The raw data were smoothed using the Savitsky–Golay algorithm provided by the instrumental software package. The detector gain (PMT voltage) was monitored for each spectrum to examine its wavelength-dependent signal-to-noise ratio.

For all proteins examined, the experimentally determined ellipticity at 208 nm (mdeg) was plotted as a function of temperature. A curve-fit to a thermodynamic model could not be carried out, because protein denaturation was irreversible and the quality of data was insufficient to use the second derivative method to estimate a thermodynamic melting temperature. Therefore, the denaturation midpoint was extracted by determining the temperature at which the ellipticity appeared to be one-half of the maximal ellipticity (after subtraction of the average ellipticity observed in the native state between 15 and 25 °C).

2.6. Thermofluor assays

All data were collected with an Applied Biosystems ABI Prism 7900HT Sequence Detection System. Samples were pipetted into the wells of 384-well polypropylene TempPlate PCR plates and covered with optically clear seals prior to data acquisition. Each well contained 20 μL of total volume with concentrations of 0.25 mg/mL cotton β-Rca, 25 mM HEPES pH 7.5, 150 mM KCl, and 16X SYPRO Orange (Invitrogen, Molecular Probes, Eugene, OR). For phosphate experiments, the contents of the 20 μL wells were the same, except that 20 mM K_2HPO_4/KH_2PO4 pH 7.5 was added and the KCl concentration was decreased to 110 mM. Prior to distribution into the wells, 1.05X premixes were made from, in order of addition, Millipore deionized water, 1 M HEPES pH 7.5, 3 M KCl, 1 M K_2HPO_4/KH_2PO4 pH 7.5 (where necessary), 5 mg/mL Cotton β-Rca and 300X SYPRO Orange (made by diluting the 5000X stock in DMSO with Millipore deionized water). To each well, 19 μL of the appropriate 1.05X premix was added followed by 1 μL of various concentrated stock solutions (e.g. ADP, ATP, $MgCl_2$, etc.). All conditions were reproduced in triplicate. Thermal denaturation runs consisted of three stages: 1) a fast ramp (~0.5 °C/s) from 25 °C to 4 °C, where the temperature was held for two minutes; 2) a slow ramp (~0.03 °C/s) from 4 °C to 80 °C holding for two minutes; 3) a fast ramp (~0.5 °C/s) down to 4 °C. Fluorescence data were collected at ~8.5 s intervals throughout each run. The fluorescence intensity of each sample at the protein "melting" transition was roughly approximated using the following equation:

$$I_{Tm} = B - 1/2(B - A)$$

where A is the minimum value prior to the fluorescence increase and B is the maximum in intensity following the increase. From these fluorescence values, corresponding "melting" temperatures were obtained.

2.7. Dynamic light scattering (DLS)

Dynamic light scattering data were collected with a DynaPro NanoStar instrument (Wyatt Technology Corp., Santa Barbara, CA) and analyzed using the software Dynamics 7.0.3.12 (Wyatt Technology Corp.). Briefly, 48 μL aliquots of 1 mg/mL cotton β-Rca in 25 mM HEPES pH 8.0 and 150 mM NaCl were added to 0.1 μm Millipore spin filters followed by 2 μL of either Millipore deionized water, 35 mM ADP, 35 mM ATP, or 70 mM $MgCl_2$. The final volume was adjusted to 70 μL with Millipore deionized water. Each sample was then spin filtered for 3 min at 3000 *g* and the filtrates were transferred to disposable UVette cuvettes (Eppendorf, Hauppauge, NY) for data collection at 4 °C. Scattered light intensity fluctuations were averaged from sixty acquisitions (5 s each) and the resulting autocorrelation functions fit via the regularization method.

The Wyatt Software provides two different methods to obtain information from samples that were not previously fractionated ("batch" experiments). The cumulants method assumes a monomodal distribution of the diffusion coefficient D_t, which determines the mean and the width of the distribution. Inversion of these values gives the reported apparent hydrodynamic radius R_h, rather than the mean and Gaussian width of R_h. When the cumulants method is used, the polydispersity (Pd) represents the standard deviation of the mean of the distribution. The second method used to analyze "batch" data is the regularization method. This method assumes a smooth underlying distribution and fits the data to numerous distributions with preference given to those that are smooth rather than spiked. Unlike cumulants, regularization can be used to resolve discrete distributions with their associated mean R_h and width. In this case, Pd is the standard deviation of the mean of each distribution, weighted by the respective mass fraction (% mass). In general, it is not possible to use regularization to discriminate between distributions of species with less than a five-fold difference in mean R_h. Although this limitation must be kept in mind when comparing DLS data of different aggregates, the regularization method provided substantially better fits than the cumulants method under all conditions tested, and was therefore used to analyze Rca self-association.

3. Results

3.1. Rca self-assembly monitored by size-exclusion chromatography

Using size-exclusion HPLC (SE-HPLC), we have examined the size distribution profiles of *A. thaliana* β-Rca as a function of protein concentration in the presence of ADP, phosphate and magnesium ions. For this work, the Y53A variant was utilized, as this protein was readily available due to its high expression levels. The biophysical characteristics of Rca-Y53A, such as size polydispersity, appeared to be identical to wild-type protein. Using a standard curve, the molecular mass was estimated for the peak position of each protein band, and utilized to calculate approximate subunit stoichiometries for eluting Rca assemblies. The relative standard error in mass determinations ranged from 20 to 30% with 25% most frequently observed, indicating that the true mass of a nominal eight-subunit assembly may lie between the masses of a hexamer and a decamer. Consistent with previous reports [6,13,33], the observed self-association state was found to strongly depend on the protein concentration of the injected sample. Also as shown previously, all SE-HPLC elution profiles consisted of non-Gaussian bands with a long, trailing downslope, consistent with a broad spread of different protein populations with a variety of subunit stoichiometries (Fig. 2).

3.1.1. The coexistence of multiple assembly intermediates hinders the isolation of specific oligomeric states

Although successive sample dilutions led to the observation of numerous oligomeric states, all species larger than dimers exhibited an asymmetric peak shape (Fig. 2A). For example, injection of 260 μM Rca provided an elution band consistent with a 47-subunit aggregate at the position of the apex, whereas samples diluted to 130, 65, 6.5, and 0.65 μM Rca provided elution peaks consistent with 30, 20, 9, and 5-subunit aggregates (Fig. 2A). Notably, the position of the band apex was not only a function of sample concentration but also of volume, as half the injection volume reduces the nominal stoichiometry from 47 (Fig. 2A) to 28 (Fig. 2C). This feature indicated that protein interactions with the column stationary phase modulate the degree of subunit association.

To further examine the dynamic nature of Rca oligomerization, fractions were collected after injection of a 260-μM sample (Fig. 2A, green chromatogram) and re-injected after a 2-h incubation at 4 °C (Fig. 2B). In this experiment, the peak fraction eluting as a nominal 47-mer in the first HPLC run eluted as a 12-mer upon reinjection, the nominal 40-mer eluted as an 8-mer upon reinjection, the nominal 30-mer as a 6-mer, and the nominal 20-mer as a 4-mer (Fig. 2A, B). These results indicate that the dilution-induced disassembly process does not allow for the isolation of specific oligomers by simple column fractionation. Rather, the 20-fold sample dilution inherent to each HPLC run (Fig. 2C) causes partial on-column disassembly, which is continued by off-column disassembly in the collection tube until full equilibration is reached. Subsequent re-injection provides for additional dilution, resulting in further subunit dissociation.

3.1.2. Rca self-assembly may involve dimeric intermediates

Upon initial SE-HPLC analysis, all samples appeared to include a dimeric form (Fig. 2A, C). By mass, the fractional contribution of the dimer was judged to be roughly equal irrespective of sample dilution, suggesting that protein preparations comprised a fixed population of subunits unable to self-associate beyond the dimeric stage. In some cases, tetrameric, hexameric and octameric states were observed upon reinjection (Fig. 2B), supporting an assembly mechanism that may proceed in 2-subunit increments. Interestingly, dimeric forms appeared to be largely eliminated by SE-HPLC fractionation (Fig. 2B), suggesting that not all dimers participate in dynamic exchange reactions with higher-order oligomers.

3.1.3. Observation of non-equilibrium states

Upon elution from the column, the more highly aggregated states appeared to disassemble in a continuous fashion, providing for a trailing downslope consistent with non-equilibrium conditions. For this reason, SE-HPLC could not be utilized to estimate subunit dissociation constants. The nominal assembly states observed at the apex of eluting bands indicated significantly higher subunit stoichiometries than would be expected from recent equilibrium solution experiments based on molecular diffusion [37]. For example, upon injection of a 26 μM sample, the elution volume of the peak fraction was consistent with a 14-subunit assembly, although this fraction contained a subunit concentration of only 1.3 μM in the collection tube. However, based on the recent measurement of diffusion coefficients, a 1.3 μM Rca solution was predicted to consist of only monomers and dimers in the presence of ADP [37], providing support for the notion that the observed 14-mer did not represent an equilibrium state (Fig. 2C). Therefore, disassembly was judged to be incomplete during column elution, likely due to interactions with the porous resin surface.

3.2. Rca self-association monitored by dynamic light scattering

To examine protein assembly and aggregation under near-equilibrium conditions, DLS experiments were carried out on cotton

β-Rca-378AC, a variant bearing an Ala-Cys insert following residue 378 of the 380-residue protein [35]. This protein was examined in the absence of nucleotides or divalent cations (apo-protein), as well as in the presence of ADP, ATP, or $MgCl_2$ in pH 8 buffer containing 150 mM NaCl. Regardless of the buffer system used, DLS data indicated that Rca assembly states were highly dependent on protein concentration (data not shown), as observed by SE-HPLC. Higher protein concentrations favored increasingly larger assemblies with size distributions that displayed increasingly larger polydispersity (Pd) values and were often multimodal. In general, DLS size estimates are of lower accuracy for highly polydisperse and multimodal samples with distributions of hydrodynamic radii (R_h), because the autocorrelation function reflects the sum of each contributing exponential time constant. To resolve discrete distributions, individual species must exhibit at least a five-fold difference in R_h, or multimodal distributions are not reproducible. For these reasons, exact assembly stoichiometries could not be determined for Rca by this method. Regardless, several significant conclusions can be drawn from the DLS data (see below).

3.2.1. Apo-Rca assembles to form oligomers with low subunit stoichiometry

Surprisingly, the size distribution of apo-Rca demonstrated significantly lower polydispersity than Rca combined with nucleotides, $MgCl_2$, or both (Fig. 3). At 16 μM subunit concentration (0.70 mg/ml), the major species (80%–90%) observed for apo-Rca provided a calculated mass consistent with assemblies containing 2–4 subunits (subunit MW = 42,459 kDa) with low polydispersity (about 10%). The remaining material consisted of very large aggregates, with estimated diameters that approached or exceeded the 0.1 μm pore size of the spin filters used to prepare the samples. These aggregates were consistently observed in all DLS profiles of Rca, yet were absent in the DLS profiles of control proteins (i.e. bovine serum albumin, lysozyme) filtered in the same manner. This observation suggested rapid re-equilibration of filtrates to regenerate larger Rca assemblies, a process that appeared to occur with both apo-protein and with Rca preparations containing additives, suggesting that the aggregation mechanism may be intrinsic to Rca. Re-examination of apo-Rca after two days and one week storage at 4 °C demonstrated that the initially observed discrete distributions had collapsed to a continuous, monomodal distribution with high polydispersity (~70%), indicating continuous aggregation over time (Fig. 3B). These studies demonstrated that Rca has a strong propensity towards self-association even in the absence of nucleotides and Mg^{2+}. In fact, the absence of nucleotides has been reported to decrease the thermostability of Rca preparations [13].

3.2.2. Complexation with nucleotides and magnesium increases the degree of self-association of Rca

Cotton β-Rca treated with ADP, ATP or $MgCl_2$ showed multimodal DLS distributions with %Pd much larger than that observed for the apo protein (Fig. 3C, D, E). This observation is consistent with previous data indicating that the presence of nucleotides and Mg^{2+} increase Rca self-association [6,33]. Interestingly, 2 mM Mg^{2+} caused substantial aggregation even in the absence of nucleotides. Given the relatively low pI (<5) of Rca, this Mg^{2+} effect may reflect aggregation caused by the interaction of divalent cations with surface-exposed acidic residues.

3.3. Thermostability monitored by circular dichroism spectroscopy

To assess the thermostability of Rca from different plant species, we carried out CD experiments on a series of β-Rca proteins derived from tobacco (Fig. 4A, B), cotton (Fig. 4C), creosote (Fig. 4D), and *Arabidopsis*. The CD data for *A. thaliana* β-Rca were published previously [13]. SE-HPLC was utilized to buffer-exchange samples into 50 mM phosphate pH 7.2, 1 mM $MgSO_4$ and 0.1 mM ADP, and the apex of the eluting protein band was used for CD experiments carried out on the same day (Fig. 2D).

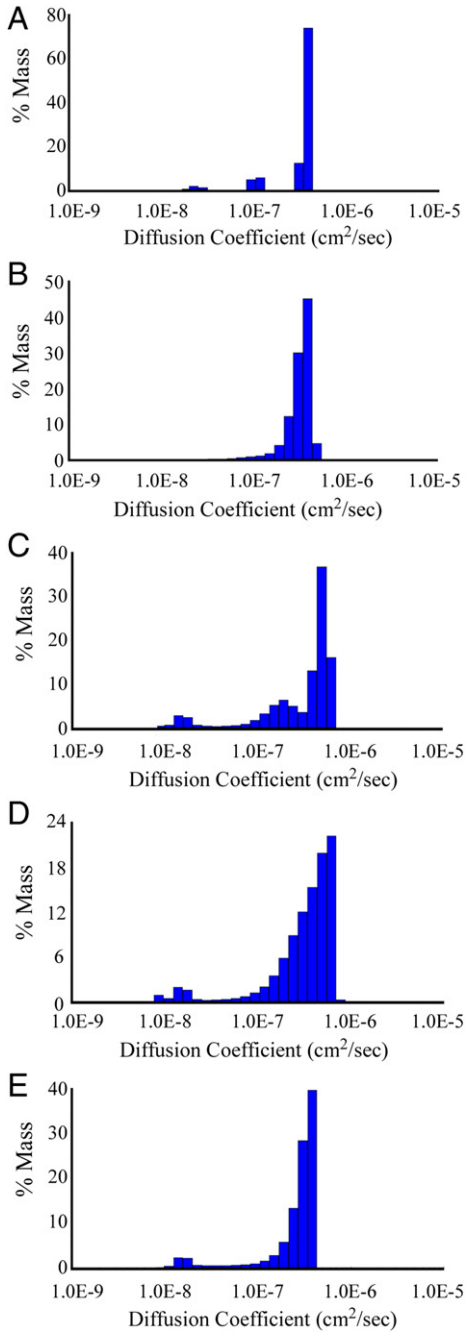

Fig. 3. DLS histograms for cotton β-Rca in the presence of various additives. A. Apo-protein; B. apo-protein after 1 week storage at 4 °C (same sample as in A); C. Rca with 1 mM ADP; D. Rca with 1 mM ATP; E. Rca with 2 mM $MgCl_2$.

CD spectral scans were collected from 185 to 250 nm, with the temperature ranging from 15 to 75 °C (Fig. 4A). Heat-induced protein denaturation proved to be irreversible in all cases, and substantial protein aggregation was observed upon cooling. Therefore, the midpoint for protein denaturation (apparent T_m) was approximated by visual inspection of ellipticity vs. temperature plots (Fig. 4B, C, D). In this way, the apparent midpoints for thermal denaturation were estimated to lie at 45 °C, 45 °C, and 46–47 °C for cotton, tobacco and creosote β-Rca, respectively (Table 1). In comparison, the apparent T_m for *A. thaliana* was significantly lower at about 40 °C [13], clearly indicating that Rca proteins from plant species adapted to hot climates are more thermostable than their Northern cousins.

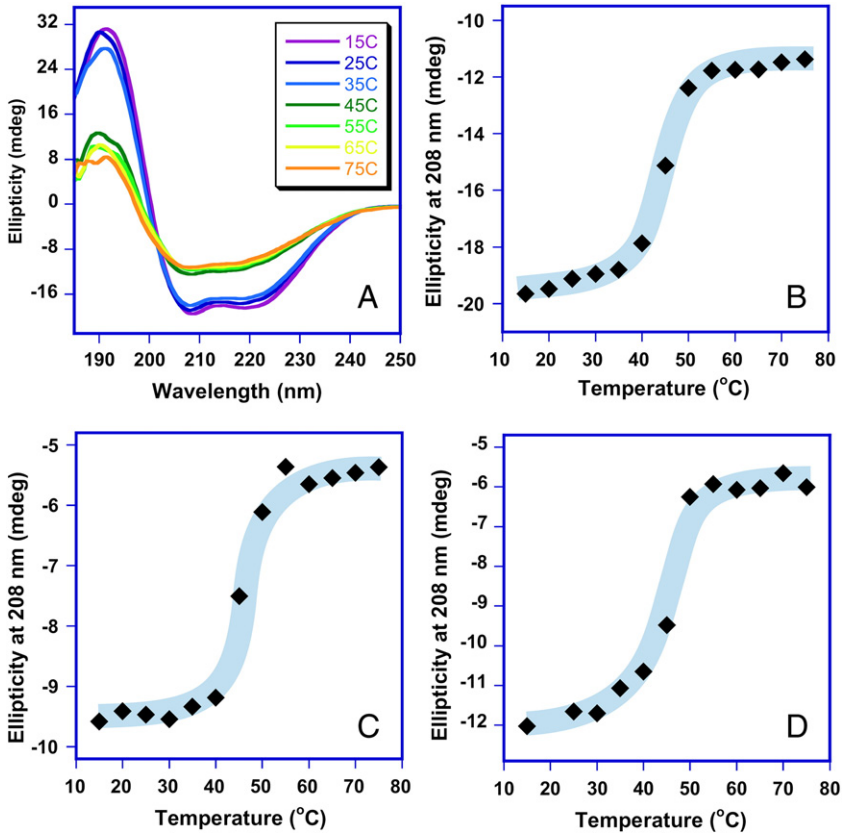

Fig. 4. A, CD wavelength scans collected on tobacco Rca; B–D, ellipticity at 208 nm plotted as a function of temperature (the blue curves are hand-drawn to provide visual guidance only); B, tobacco Rca; C, cotton β-Rca; D, creosote β-Rca.

In a separate set of experiments, the thermostability of the redox-responsive α-Rca proteins from creosote and spinach were also examined. Although the CD spectra were consistent with the native structure as indicated by a high α-helical content, α-Rcas did not provide high-quality CD scans at wavelengths shorter than 210 nm. This observation suggests significant protein aggregation even under room temperature conditions. Upon moderate heating to 35 °C, the thermal scans provided evidence of heavily aggregated protein, such that a sigmoidal melting curve could not be extracted. Therefore, the T_m for protein denaturation could not be estimated for any α-Rca proteins examined to date.

3.4. Nucleotide, magnesium and phosphate binding monitored by the Thermofluor assay

To assess the effects of nucleotide, magnesium and phosphate, the thermal stability of cotton β-Rca as a function of additives was examined by the Thermofluor assay [38]. In this assay, the heat-induced exposure of protein hydrophobic groups causes a fluorescence increase of the dye SYPRO Orange, until a sharp loss of fluorescence is observed at even higher temperatures (Fig. 5). Although the thermodynamic denaturation temperature of the protein cannot be extracted by this method, the Thermofluor assay allows for the rapid comparison of apparent T_m values under different buffer conditions.

Table 1
Comparison of in vitro thermal profiles and natural habitat of higher plant Rca proteins.

Rca protein	Maximum ATPase activity [5,17]	Onset of protein denaturation	Apparent T_m (CD)	Natural habitat climate
Hairgrass	27°	–	–	Antarctic
Spinach α	25°	–	–	Northern temperate
Arabidopsis β		~32°	~40°	Northern temperate
Cotton β	33°	~40°	~45°	Sub-tropical
Tobacco	35°	~40°	~45°	Tropical
Creosote β	35°	~40°	~46–47°	Deserts

3.4.1. ADP-complexation increases the thermal stability of Rca over ATP-binding

Apo-protein preparations of Rca demonstrated a strong increase in fluorescence upon heating (Fig. 5A–C) with an estimated T_m value of 37.4 ± 0.8 °C (Table 2). Titration with increasing amounts of ADP caused a continuous rise of the apparent T_m up to 50.0 ± 0.4 °C at 8 mM ADP, the highest ADP concentration tested (Fig. 5A; Table 2). By contrast, the stability imparted by ATP binding appeared less significant, as 8 mM ATP increased the apparent T_m to only 42.2 ± 0.2 °C (Fig. 5B). The difference in the relative stabilities of ADP- and ATP-bound Rca proved consistent with previous K_d measurements for nucleotide complexation that indicated tighter association of ADP than ATP [11,39], in line with a nucleotide pocket that is particularly well-suited for ADP binding, but less so for ATP binding.

3.4.2. Magnesium increases the thermal stability of ATP-bound, but destabilizes ADP-bound Rca

ATP and (to a lesser degree) ADP are known to associate with Mg^{2+} in solution and within the active sites of many nucleotide-binding proteins. Therefore, the apparent T_m of cotton β-Rca was measured as a function of increasing $MgCl_2$ concentrations, and also as a function of increasing ATP and ADP concentrations with a constant 1 mM excess of Mg^{2+} over nucleotide. In the absence of nucleotides, Mg^{2+} concentrations greater than

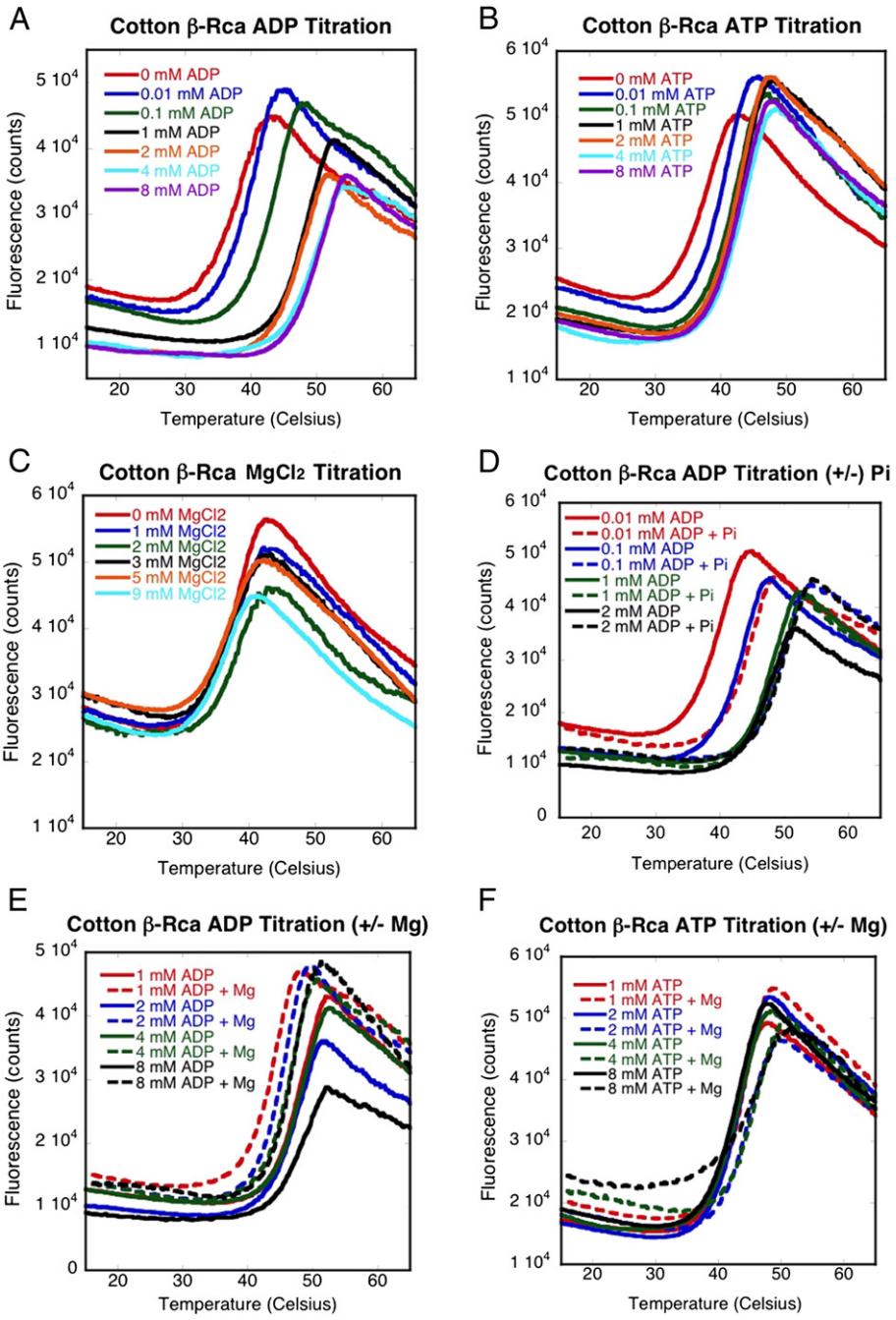

Fig. 5. Thermofluor assays. A. ADP titration; B. ATP titration; C. $MgCl_2$ titration; D. ADP titration in the presence or absence of 20 mM phosphate (P_i); E. ADP titration with and without 1 mM excess of $MgCl_2$ (Mg); F. ATP titration with and without 1 mM excess $MgCl_2$ (Mg).

2 mM appeared to have a slightly destabilizing effect of about 1 °C (Table 2, Fig. 5C). However, in the presence of 1 mM ADP, 2 mM Mg^{2+} destabilized Rca by a striking 6 °C, whereas in the presence of 1–4 mM ATP, 2–5 mM Mg^{2+} caused mild protein stabilization by about 1.3–2.7 °C (Fig. 5E, F). Hence, the differential Mg^{2+} effect demonstrates a strong dependence on the number of phosphates attached to the nucleoside, suggesting that electrostatic effects within the nucleotide-binding pocket may play a role in modulating stability. Perhaps the presence of divalent Mg^{2+} counterbalances the larger negative charge associated with bound ATP, thus reducing the loss of stability when ADP is replaced with ATP. The Thermofluor results are consistent with the reported K_d values on tobacco Rca indicating tighter binding of Mg·ATP than ATP [39]. In the ADP-bound state, divalent cations may interact with Rca elsewhere on the protein's surface, causing a loss in stability by facilitating protein aggregation.

3.4.3. Phosphate increases the thermal stability of ADP-bound Rca

The role of phosphate in the thermal stabilization of ADP-bound Rca was tested by adding 20 mM KH_2PO_4/K_2HPO_4 pH 7.5 to protein titrated with ADP alone or titrated with ADP plus a 1 mM excess of Mg^{2+}. In the absence of Mg^{2+}, phosphate exerted a stabilizing effect on ADP-bound Rca, particularly at lower ADP concentrations (0.01–2 mM) (Table 2, Fig. 5D). At the lowest ADP concentration examined (0.01 mM), the increase in T_m appeared largest (+2.4 °C). Upon addition of Mg^{2+} to ADP-bound Rca, protein stability was reduced, particularly at 1 mM ADP, the lowest concentration tested (+2.6 °C). Perhaps phosphate

Table 2
Thermofluor data for cotton β-Rca.

ADP (mM)	ATP (mM)	Mg^{2+} (mM)	P_i* (mM)	Apparent T_m (°C ± std. dev.)
–	–	–	–	37.4 ± 0.8
0.01				38.8 ± 0.6
0.1				43.1 ± 0.5
1				47.6 ± 0.2
2				47.2 ± 0.6
4				49.1 ± 0.3
8				50.0 ± 0.4
	0.01			39.7 ± 0.4
	0.1			41.5 ± 0
	1			42.3 ± 0
	2			42.2 ± 0.8
	4			42.5 ± 0.3
	8			42.2 ± 0.2
		1		37.4 ± 0.5
		2		37.1 ± 0.8
		3		36.7 ± 0.3
		5		36.4 ± 0.4
		9		36.1 ± 0.5
0.01			20	41.2 ± 0.2
0.1			20	44.0 ± 0.3
1			20	49.3 + 0.9
2			20	48.2 ± 0.3
4			20	49.5 ± 0.3
8			20	49.9 ± 0.1
1		2		41.4 ± 0.5
2		3		44.9 ± 0.6
4		5		46.3 ± 0.4
8		9		47.7 ± 0.1
	1	2		43.6 ± 0
	2	3		44.3 ± 0.2
	4	5		45.2 ± 0.3
	8	9		44.7 ± 0.7
1		2	20	44.0 ± 0.2
2		3	20	45.1 ± 0.3
4		5	20	46.6 ± 0.7
8		9	20	48.5 ± 0.2

* Note: 20 mM K_2HPO_4/KH_2PO_4 at pH 7.5 (P_i) was included in some of the samples as part of the premix before additive addition. In these cases, the KCl content of the premix was lowered to keep the ionic strength constant.

binding to ADP-complexed Rca favors an active site conformation identical to that induced by nucleotide hydrolysis prior to phosphate release. Alternatively, the stabilizing effect may result from unknown protein–phosphate interactions away from the nucleotide binding pocket. Interestingly, magnesium ions appeared to destabilize ADP-bound Rca irrespective of the presence or absence of phosphate.

3.4.4. Summary of nucleotide, magnesium and phosphate effects

When comparing apparent T_m values measured at 1 mM nucleotide, ±2 mM Mg^{2+} and ±20 mM P_i, the results may be summarized as follows. ADP stabilizes the apo-protein by 10 °C, whereas ATP stabilizes the apo-protein by only 5 °C. Mg^{2+} alone does not modify the stability of the apo-protein, however, Mg^{2+} destabilizes the ADP-bound form by 6 °C and stabilizes the ATP-bound form by 1 °C. P_i stabilizes the ADP-bound form by 2 °C, and stabilizes the Mg^{2+} and ADP-bound form by 3 °C, thus partially compensating for the destabilizing magnesium effect. Based on these results, we hypothesize that P_i occupies the active site adjacent to ADP, whereas Mg^{2+} binds at a remote site on the protein surface that is accessible in the ADP-bound but not ATP-bound form of Rca, and reduces thermal stability.

4. Discussion

A number of studies have provided evidence that the CO_2-fixing enzyme system Rubisco/Rubisco activase embodies a primary limiting factor of net photosynthesis under heat stress conditions. This restriction on carbon fixation in higher plants has been proposed to be due to a temperature-dependent loss of Rca hydrolytic activity [5]. To better assess the potential for structure-guided genetic engineering of Rca to identify more thermostable variants with appropriate Rubisco specificity, we have characterized the in vitro thermal denaturation profiles of higher plant Rca proteins. All CD thermal melts were consistent with highly temperature-sensitive proteins. The most heat-resistant Rca identified in our study was creosote β-Rca with a T_m of 46–47 °C, closely followed by tobacco Rca with a T_m of 45 °C (Table 1). Perhaps it is no coincidence that to date, the only Rca X-ray structures available are those of creosote and tobacco Rca [27,28]. In general, a clear increase in the midpoint for protein denaturation was observed when moving from Northern temperate to subtropical and tropical to desert environments, indicating that plants from cooler climates have Rca proteins with lower T_m than those from warmer climates. The thermal profiles follow reported activity data demonstrating that the temperature of maximal hydrolytic turnover increases from 25 to 35 °C when comparing spinach with creosote and tobacco Rca [5,17].

Frequently, substrate, inhibitor, and cofactor binding lend increased thermal stability to proteins and enzymes by restricting dynamic motions of the protein fold. This mechanism may include the acquisition tertiary structure by regions of the protein that are intrinsically disordered in the absence of cofactors. In the ring-forming ATPases, differential subunit interactions with nucleotides may play a regulatory role, and magnesium ions may modulate hydrolytic activity by serving as co-substrates. In the chloroplast stoma, where the Rubisco/Rca system is located, the free Mg^{2+} concentration is thought to change as a function of light/dark adaptation in step with the available energy charge [13,40]. Notably, Mg^{2+} is also known to play an essential role in activating Rubisco [1].

To rapidly screen for Rca complexation with nucleotides, magnesium and phosphate ions, the Thermofluor assay was employed. Consistent with previously reported affinity studies [11], ADP was found to provide greater thermal stabilization than ATP. In contrast, Mg^{2+} had an overall destabilizing effect, both in the absence of nucleotides and in the presence of ADP, but appeared to be weakly stabilizing when paired with ATP. A likely explanation for this effect is an electrostatic balancing of the binding pocket upon Mg^{2+} complexation to the β- and γ- phosphoryl groups of ATP. This type of metal complexation is physiologically relevant, as it is a prerequisite for catalytic ATP hydrolysis. In contrast, when ATP is absent, excess divalent cations may bind elsewhere on the protein surface and induce non-specific protein aggregation. Although not unusual for acidic proteins such as Rca, this type of Rca aggregation remains poorly characterized. Notably, phosphate ions in the presence of low ADP concentrations demonstrated a weakly stabilizing effect, consistent with the formation of the ADP·P_i product complex in the active site.

Whether monitored by CD or Thermofluor, thermal denaturation was accompanied by irreversible protein aggregation in all cases examined. This phenomenon may be due to non-specific interactions of unstructured regions bearing exposed hydrophobic groups, leading to the formation of soluble oligomers. Subsequently, such non-native oligomeric species may further associate with each other to form high-MW disordered aggregates. These larger aggregates may or may not contain natively folded core regions, and their mode of self-association may or may not resemble native assemblies.

In spite of intense efforts by a number of researchers, the Rca assembly mechanism to functional oligomers has remained somewhat elusive. To date, the quaternary structures responsible for Rubisco reactivation remain largely unknown, although hexameric species appear to be involved [28]. To aid in elucidating the Rca self-association behavior, we have used non-equilibrium (SE-HPLC) and equilibrium (DLS) methods. We hope that this work will help resolve a long-standing puzzle in the field, as many attempts have been made to use SE-chromatography to assess Rca assembly. We have demonstrated that this method does not provide equilibrium data, and is

therefore of limited use for monitoring quaternary protein structure. On-column subunit dissociation due to sample dilution does not appear to lead to full equilibration within the timeframe of HPLC detection, and protein interactions with the molecular surface of the porous resin seem to play a significant role in the observed size distribution.

For these reasons, we resorted to DLS measurements to assess the nature of more highly equilibrated Rca self-association states. DLS provided results consistent with significant size heterogeneity and polydispersity in protein preparations, as observed by SE-HPLC. When Rca concentrations were increased incrementally, distributions with increasingly larger mean masses were observed. This feature supports a seemingly continuous Rca assembly mechanism, rather than the formation of discrete intermediates with well-defined stoichiometries and substantial size differences. A distribution of several species appears to co-exist over a broad concentration range, such that specific oligomeric states are difficult to observe directly (Fig. 3). An exception to this rule is the routine observation of dimeric species by SE-HPLC (Fig. 2A, C), suggesting that two-subunit modules may comprise the basic building block for Rca self-assembly. The concentration-dependent addition of dimers to growing Rca oligomers may lead to the formation of hexameric states by way of a transient tetrameric species (Fig. 6), as recently proposed based on fluorescence correlation spectroscopic data [37]. Subsequently, hexameric spirals may form and continue to grow along the helical axis to form large aggregates with a broad size distribution, in line with the Rca AAA+ crystallographic model [28]. The helical subunit arrangement observed in the AAA+ X-ray structure is reproduced in Fig. 6, where the pdb coordinates were utilized to generate a coarse-grained surface representation of Rca subunit interactions in the crystal. This type of supramolecular structure may form spontaneously in the test tube by the step-wise addition of either dimeric (left path) or hexameric (right path) oligomers to a growing helical fibril. In an alternative model, closed ring toroids such as shown in Fig. 1 may stack on top of each other to form larger aggregates. Both models were recently described by Chakraborty et al. based on data obtained using fluorescence fluctuation techniques [37]. We speculate that the helical arrangement is more prominent in the test tube, whereas closed toroidal assemblies are more prominent in the crowded environment of the chloroplast stroma.

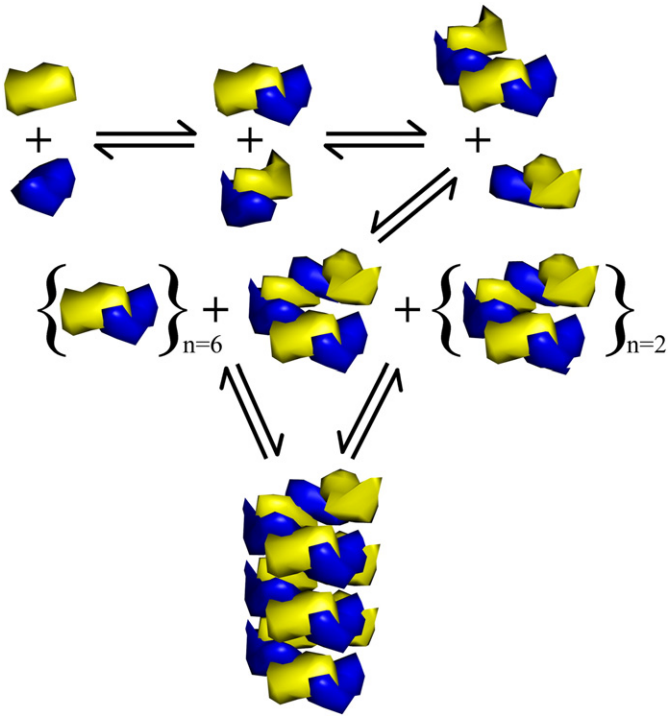

Fig. 6. Hypothetical model of the in vitro assembly of Rca from monomers (yellow and blue) to larger complexes (18 mer shown). In the first step, monomers combine to form dimers. In the second and third steps, the sequential addition of two dimers leads to a hexamer by way of a tetrameric intermediate. From here, two possible routes to higher-order assemblies are proposed, via addition of dimers (left path), or via addition of hexamers (right path). The figure was created by calculating a coarse surface representation of the crystal structure of tobacco Rca (PDB ID 3T15) using the program PyMOL.

DLS measurements of freshly prepared apo-protein indicated a markedly reduced size polydispersity, suggesting that the major component of nucleotide-free Rca may consist of an oligomer smaller than a hexamer (Fig. 3). In contrast, Rca prepared in the presence of ATP, ADP or Mg^{2+} exhibits a much larger average mass and a significantly higher percent polydispersity. This effect may reflect some type of conformational change upon nucleotide/Mg^{2+} binding that favors self-association, in line with a direct role for nucleotides in subunit assembly. Surprisingly, a difference in ADP- and ATP-mediated assembly could not be discerned by DLS, contrary to some literature reports [33]. Regardless, the specific nucleotide effects on assembly remain poorly understood, as it is currently unknown which oligomeric states of the apoprotein are most prone to time-dependent aggregation. A hypothetical but reasonable model may entail a branch point at the tetrameric state, where the presence of nucleotides may promote native assembly pathways to hexameric and higher-order forms, whereas the lack of nucleotides may promote non-native self-association pathways facilitated by partially disordered domains or subdomains, such as the Rca N- and C-terminal extension to the AAA+ domain.

Assembly into functionally active complexes upon nucleotide binding is a recurring theme among AAA+ proteins. Such complexes usually consist of closed-ring structures, most commonly hexamers, and often involve partner proteins with defined stoichiometries [41]. In the case of Rca, in vitro nucleotide-induced self-association proceeds readily in the absence of the partner enzyme Rubisco. The formation of higher-order oligomers in the presence of nucleotides and magnesium ions was observed previously for both α and β isoforms of Rca [33]. Structural studies of numerous AAA+ proteins reveal a conserved arginine residue within the N-domain termed the "arginine finger". This residue has functional resemblance to the "arginine finger" of GTPases, which interacts with the γ-phosphate of ATP bound to the adjacent protomer within oligomeric assemblies. Such interactions are believed to facilitate communication between subunits, in addition to playing a role in assembly and catalysis [23].

Mutational analysis of the "arginine finger" in spinach and tobacco Rca (Arg239 and Arg244, respectively) has demonstrated that this residue is required for ATP hydrolysis, but not for ATP binding [42]. Surprisingly, a comparison of data from wild type and mutant enzymes found an element of species specificity with regard to ATP-dependent size increases and that these increases did not necessarily correlate with ATPase activity or conformational changes inferred from intrinsic fluorescence [42]. The recently published three-dimensional structure of the AAA+ module from tobacco apo-Rca (PDB ID 3T15) does not provide a model for the Arg244 side chain beyond the β-carbon, presumably due to a lack of interpretable electron density [28]. Thus, it is difficult to assess the potential for a direct interaction between Arg244 and the ATP γ-phosphate in the adjacent protomer in the helical X-ray structure. However, a closed hexameric ring model (PDB ID 3ZW6) was also constructed by superimposing the apo-structure monomer onto the hexameric AAA+ protein p97 (PDB ID 3CF3) [28]. This structure places the Arg244 side chain within a reasonable distance of the nucleotide binding pocket in the adjacent protomer, providing some structural insight into nucleotide-mediated assembly involving the "arginine finger". Arg244 is one of several conserved arginine residues important for proper functioning of Rca. Others include Arg241, which is

also part of the N-domain BoxVII, as well as Arg294 and Arg296 located in the Sensor 2 portion of the C-domain. The roles of these residues in Rca structure and function will require the availability of X-ray structures of Rca-nucleotide complexes.

In combination, the data presented in this study will allow for the targeting of select Rca species with high thermal stability to better characterize factors governing self-association, with the ultimate goal of facilitating further biophysical studies. It appears that the slow progress towards a mechanistic and structural understanding of this key photosynthetic enzyme results from its highly thermolabile nature, in combination with its intrinsic propensity towards aggregation. Therefore, we hope that the in-depth characterization presented here will accelerate research efforts aimed at understanding the regulation of higher plant carbon fixation at elevated temperatures.

Acknowledgments

This work was supported by grants from the US Department of Energy Office of Basic Energy Sciences, Photosynthetic Systems Grant No. DE-FG02-09-ER16123 to R.M.W., and Grant No. DE-FG02-08ER-20268 to M.E.S.

References

[1] R.J. Spreitzer, M.E. Salvucci, Rubisco: structure, regulatory interactions, and possibilities for a better enzyme, Annu. Rev. Plant Biol. 53 (2002) 449–475.
[2] F.G. Pearce, T.J. Andrews, The relationship between side reactions and slow inhibition of ribulose-bisphosphate carboxylase revealed by a loop 6 mutant of the tobacco enzyme, J. Biol. Chem. 278 (2003) 32526–32536.
[3] I. Andersson, Catalysis and regulation in Rubisco, J. Exp. Bot. 59 (2008) 1555–1568.
[4] Z.Y. Wang, A.R.J. Portis, Dissociation of ribulose-1,5-bisphosphate bound to ribulose-1,5-bisphosphate carboxylase/oxygenase and its enhancement by ribulose-1,5-bisphosphate carboxylase/oxygenase activase-mediated hydrolysis of ATP, Plant Physiol. 99 (1992) 1348–1353.
[5] S.J. Crafts-Brandner, M.E. Salvucci, Rubisco activase constrains the photosynthetic potential of leaves at high temperature and CO2, Proc. Natl. Acad. Sci. U. S. A. 97 (2000) 13430–13435.
[6] A.R. Portis, Rubisco activase – Rubisco's catalytic chaperone, Photosynth. Res. 75 (2003) 11–27.
[7] A.R.J. Portis, C. Li, D. Wang, M.E. Salvucci, Regulation of Rubisco activase and its interaction with Rubisco, J. Exp. Bot. 59 (2008) 1597–1604.
[8] T.C. Taylor, I. Andersson, Structural transitions during activation and ligand binding in hexadecameric Rubisco inferred from the crystal structure of the activated unliganded spinach enzyme, Nat. Struct. Biol. 3 (1996) 95–101.
[9] A.P. Duff, T.J. Andrews, P.M.G. Curmi, The transition between the open and closed states of Rubisco is triggered by the inter-phosphate distance of the bound bisphosphate, J. Mol. Biol. 2000 (2000) 903–916.
[10] N. Zhang, R.P. Kallis, R.G. Ewy, A.R.J. Portis, Light modulation of Rubisco in Arabidopsis requires a capacity for redox regulation of the larger Rubisco activase isoform, Proc. Natl. Acad. Sci. 99 (2002) 3330–3334.
[11] D. Wang, A.R.J. Portis, Two conserved tryptophan residues are responsible for intrinsic fluorescence enhancement in Rubisco activase upon ATP binding, Photosynth. Res. 88 (2006) 185–193.
[12] M.E. Salvucci, F.J. van de Loo, D. Stecher, Two isoforms of Rubisco activase in cotton, the products of separate genes not alternative splicing, Planta 216 (2003) 736–744.
[13] C. Barta, A.M. Dunkle, R.M. Wachter, M.E. Salvucci, Structural changes associated with the acute thermal instability of Rubisco activase, Arch. Biochem. Biophys. 499 (2010) 17–25.
[14] C. Barta, A.E. Carmo-Silva, M.E. Salvucci, Purification of Rubisco activase from leaves or after expression in Escherichia coil, in: R. Carpentier (Ed.), Photosynthesis Research Protocols Second edition, 2011, pp. 363–374, vol. 684.
[15] R. Zhang, J.A. Cruz, D.M. Kramer, M.E. Magallanes-Lundback, D. Dellapenna, T.D. Sharkey, Moderate heat stress reduces the pH component of the transthylakoid proton motive force in light-adapted, intact tobacco leaves, Plant Cell Environ. 32 (2009) 1538–1547.
[16] T.D. Sharkey, R. Zhang, High temperature effects on electron and proton circuits of photosynthesis, J. Integr. Plant Biol. 52 (2010) 712–722.
[17] M.E. Salvucci, S.J. Crafts-Brandner, Relationship between the heat tolerance of photosynthesis and the thermal stability of rubisco activase in plants from contrasting thermal environments, Plant Physiol. 134 (2004) 1460–1470.
[18] A.F. Neuwald, L. Aravind, J.L. Spouge, E.V. Koonin, AAA+: a class of chaperone-like ATPases associated with the assembly, operation, and disassembly of protein complexes, Genome Res. 9 (1999) 27–43, www.genome.org.
[19] A.N. Lupas, J. Martin, AAA proteins, Curr. Opin. Struct. Biol. 12 (2002) 746–753.
[20] L.M. Iyer, D.D. Leipe, E.V. Koonin, L. Aravind, Evolutionary history and higher order classification of AAA+ ATPases, J. Struct. Biol. 146 (2004) 11–31.
[21] G.R. Smith, B. Contreras-Moreira, X. Zhang, P.A. Bates, A link between sequence conservation and domain motion within the AAA+ family, J. Struct. Biol. 146 (2004) 189–204.
[22] M. Ammelburg, T. Frickey, A.N. Lupas, Classification of AAA+ proteins, J. Struct. Biol. 156 (2006) 2–11.
[23] J. Snider, W.A. Houry, AAA+ proteins: diversity in function, similarity in structure, Biochem. Soc. Trans. 36 (2008) 72–77.
[24] M. Bochtler, C. Hartmann, H.K. Song, G.P. Bourenkov, H.D. Bartunik, R. Huber, The structures of HslU and the ATP-dependent protease HslU–HslV, Nature 403 (2000) 800–805.
[25] G.L. Hersch, R.E. Burton, D.N. Bolon, T.A. Baker, R.T. Sauer, Asymmetric interactions of ATP with the AAA+ ClpX6 unfoldase: allosteric control of a protein machine, Cell 121 (2005) 1017–1027.
[26] D.M. Smith, H. Fraga, C. Reis, G. Kafri, A.L. Goldberg, ATP binds to proteasomal ATPases in pairs with distinct functional effects, implying an ordered reaction cycle, Cell 144 (2011) 526–538.
[27] J.N. Henderson, A.M. Kuriata, R. Fromme, M.E. Salvucci, R.M. Wachter, Atomic resolution X-ray structure of the substrate recognition domain of higher plant ribulose-bisphosphate carboxylase/oxygenase (Rubisco) activase, J. Biol. Chem. 286 (2011) 35683–35688.
[28] M. Stotz, O. Mueller-Cajar, S. Ciniawsky, P. Wendler, F.U. Hartl, A. Bracher, M. Hayer-Hartl, Structure of green-type Rubisco activase from tobacco, Nat. Struct. Mol. Biol. 18 (2011) 1366–1370.
[29] C. Li, M.E. Salvucci, A.R.J. Portis, Two residues of Rubisco activase involved in recognition of the Rubisco substrate, J. Biol. Chem. 280 (2005) 24864–24869.
[30] J.J. Hartman, R.D. Vale, Microtubule disassembly by ATP-dependent oligomerization of the AAA enzyme katanin, Science 286 (1999) 782–785.
[31] D.A. Hattendorf, S.L. Lindquist, Cooperative kinetics of both Hsp104 ATPase domains and interdomain communication revealed by AAA sensor-1 mutants, EMBO J. 21 (2002) 12–21.
[32] W. Kress, H. Mutschler, E. Weber-Ban, Assembly pathway of an AAA+ protein: tracking ClpA and ClpAP complex formation in real time, Biochemistry 46 (2007) 6183–6193.
[33] Z.Y. Wang, R.T. Ramage, A.R.J. Portis, Mg^{2+} and ATP or adenosine 5′-[γ-thio]-triphosphate (ATPγS) enhances intrinsic fluorescence and induces aggregation which increases the activity of spinach Rubisco activase, Biochim. Biophys. Acta 1202 (1993) 47–55.
[34] M.J. Blayney, S.M. Whitney, J.L. Beck, NanoESI mass spectrometry of Rubisco and Rubisco activase structures and their interactions with nucleotides and sugar phosphates, J. Am. Soc. Mass Spectrom. 22 (2011) 1588–1601.
[35] M.E. Salvucci, Potential for interactions between the carboxy- and amino-termini of Rubisco activase subunits, FEBS Lett. 560 (2004) 205–209.
[36] H.S. Penefsky, Reversible binding of Pi by beef heart mitochondrial adenosinetriphosphatase, J. Biol. Chem. 252 (1977) 2891–2899.
[37] M. Chakraborty, A.M. Kuriata, J.N. Henderson, M.E. Salvucci, R.M. Wachter, M. Levitus, Protein Oligomerization Monitored by Fluorescence Fluctuation Spectroscopy: Self-Assembly of Rubisco Activase, Biophys. J. 103 (2012) 949–958.
[38] U.B. Ericsson, B.M. Hallberg, G.T. DeTitta, N. Dekker, P. Nordlund, Thermofluor-based high-throughput stability optimization of proteins for structural studies, Anal. Biochem. 357 (2006) 289–298.
[39] F.J. van de Loo, M.E. Salvucci, Involvement of two aspartate residues of Rubisco activase in coordination of the ATP-γ-phosphate and subunit cooperativity, Biochemistry 37 (1998) 4621–4625.
[40] S. Ishijima, A. Uchibori, H. Takagi, R. Maki, M. Ohnishi, Light-induced increase in free Mg^{2+} concentration in spinach chloroplasts: measurement of free Mg^{2+} by using a fluorescent probe and necessity of stromal alkalinization, Arch. Biochem. Biophys. 412 (2003) 126–132.
[41] J.P. Erzberger, J.M. Berger, Evolutionary relationships and structural mechanisms of AAA plus proteins, Annu. Rev. Biophys. Biomol. Struct. 35 (2006) 93–114.
[42] C. Li, D. Wang, A.R.J. Portis, Identification of critical arginine residues in the functioning of Rubisco activase, Arch. Biochem. Biophys. 450 (2006) 176–182.